Chemical Science

ROYAL SOCIETY OF CHEMISTRY

EDGE ARTICLE

View Article Online
View Journal | View Issue

Cite this: *Chem. Sci.*, 2021, **12**, 4154

All publication charges for this article have been paid for by the Royal Society of Chemistry

Establishing plasmon contribution to chemical reactions: alkoxyamines as a thermal probe†

Olga Guselnikova, [a] Gérard Audran,[b] Jean-Patrick Joly,[b] Andrii Trelin,[c] Evgeny V. Tretyakov,[d] Vaclav Svorcik,[c] Oleksiy Lyutakov, [c] Sylvain R. A. Marque *[b] and Pavel Postnikov *[ac]

Received 25th November 2020
Accepted 22nd January 2021

DOI: 10.1039/d0sc06470j

rsc.li/chemical-science

The nature of plasmon interaction with organic molecules is a subject of fierce discussion about thermal and non-thermal effects. Despite the abundance of physical methods for evaluating the plasmonic effects, chemical insight has not been reported yet. In this contribution, we propose a chemical insight into the plasmon effect on reaction kinetics using alkoxyamines as an organic probe through their homolysis, leading to the generation of nitroxide radicals. Alkoxyamines (TEMPO- and SG_1-substituted) with well-studied homolysis behavior are covalently attached to spherical Au nanoparticles. We evaluate the kinetic parameters of homolysis of alkoxyamines attached on a plasmon-active surface under heating and irradiation at a wavelength of plasmon resonance. The estimation of kinetic parameters from experiments with different probes (**Au–TEMPO**, **Au–SG_1**, **Au–SG_1–TEMPO**) allows revealing the apparent differences associated with the non-thermal contribution of plasmon activation. Moreover, our findings underline the dependency of kinetic parameters on the structure of organic molecules, which highlights the necessity to consider the nature of organic transformations and molecular structure in plasmon catalysis.

Introduction

Plasmon-driven chemistry is a rapidly developing area, where existing limitations of heterogeneous catalysis, such as high temperature and pressure and utilization of an elaborated catalyst, can be overcome.[1–9] Plasmonic chemistry also offers endless opportunities for the discovery of new reaction pathways. Nevertheless, the mechanism of interaction between a plasmon and organic molecules is still the subject of global debate.[10–16] Some groups postulate the dominant role of heating effects,[10,11] and others are convinced that the transfer of hot carriers or intramolecular excitation of electrons is the rate-determining step.[17–19] In particular, photoexcitation generates free charged carriers or excites the molecule in the surrounding medium (a non-thermal effect). At the same time, hot carrier relaxation through electron–phonon scattering leads to the heating of the surrounding media (a thermal effect). Both mechanisms can contribute to the catalytic activity of plasmonic nanostructures. Recent studies address the challenge of disentangling thermal from non-thermal effects; however, the relative importance of each effect remains an issue under fierce debate.[17,20–24] Previous reports are focused on the quantification of thermal and non-thermal effects mostly using physical approaches and instruments.[20–22] However, physical approaches offer only a partial solution to this problem due to the lack of knowledge regarding the chemical structure and reactivity patterns of reacting compounds.

What if, to bring up a different perspective, the aforementioned issue can be resolved from an alternative chemical point of view. The utilization of molecules with known and predictable reactivity under heating as a chemical probe may open a new opportunity for determining the impact of each thermal and non-thermal effect. This is especially true in terms of reaction kinetics, one of the main tools to gain more in-depth insights into plasmon catalysis.[25] Nowadays, the kinetic studies of plasmonic chemistry are commonly performed using dimerization reactions with the formation of azo-moieties from anilines or nitroarenes, transformation of Amplex Red to resorufin, and oxidation of dyes[26–29] (Fig. 1). In these cases, the kinetic investigations are hampered by the involvement of the second component (*e.g.*, oxygen in the case of azo-moiety formation), which leads to second-order kinetic curves.[30] These interfering factors distort the output kinetic data due to the diffusion effects, molecule collision, and reagent concentration.

[a]*Research School of Chemistry and Applied Biomedical Sciences, Tomsk Polytechnic University, Russian Federation. E-mail: postnikov@tpu.ru*

[b]*Aix-Marseille Univ, CNRS, ICR case 551, Avenue Escadrille Normandie-Niemen, 13397 Marseille Cedex 20, France. E-mail: sylvain.marque@univ-amu.fr*

[c]*Department of Solid-State Engineering, University of Chemistry and Technology, Prague, Czech Republic*

[d]*N.D. Zelinsky Institute of Organic Chemistry, Leninsky Prospect, 47, Moscow 119991, Russia*

† Electronic supplementary information (ESI) available. See DOI: 10.1039/d0sc06470j

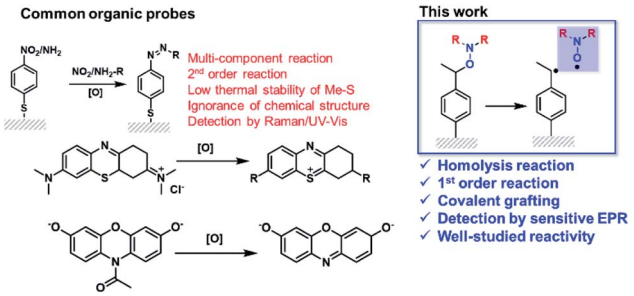

Fig. 1 Comparison of previously reported organic probes with alkoxyamines attached to the surface for mechanistic evaluation of plasmonic chemistry.

Also, the primary source of information about the conversion of reacting compounds in plasmon-assisted reactions is still Raman spectroscopy.[26–29]

On the other hand, the on-surface homolysis of functional groups seems to be more favorable for the in-depth analysis of kinetics in the case of plasmon-catalyzed reactions (Fig. 1). First of all, the homolysis processes represent first-order and one-stage transformations without additional reagents, excluding most of the interfering factors. Not less important is the fact that the reaction leads to the formation of easy-to-detect products – stable nitroxide radicals (Fig. 1). In contrast to other short-living species, stable radicals can be precisely detected and monitored by electron paramagnetic resonance, blind to the spin-neutral molecules.

Recently, we demonstrated the possibility of plasmon-driven NO–C bond homolysis in alkoxyamines, which were covalently attached to a plasmon-active surface.[31] NO–C bond homolysis leads to nitroxyl radical formation (1st order, one component reaction) followed by surface-initiated nitroxide-mediated polymerization.[32] The number of generated radicals can be precisely and quickly determined by common electron paramagnetic resonance (EPR) spectroscopy. Moreover, the homolysis of alkoxyamines proceeds with the formation of a benzyl-type carbon-centered radical and nitroxide at elevated temperatures (~100 °C is often required). The exact temperature strongly depends on the structure of the alkoxyamine.[33] The well-investigated structure–reactivity relationship for alkoxyamines provides the possibility to compare thermal and non-thermal effects.

In this contribution, we present a novel approach to exploring the thermal and non-thermal effects of a plasmon using alkoxyamines as chemical probes. To obtain a holistic picture, we demonstrated the behavior of well-studied alkoxyamines covalently grafted onto plasmonic AuNPs under illumination as a model system. All batches of covalently modified AuNPs were standardized using Au concentration, absorption coefficients, and alkoxyamine loadings. The difference in the kinetics of C–ON bond homolysis in alkoxyamines under heating and illumination enabled us to establish the presence of a non-thermal component and the critical role of the molecular structure in the observed plasmonic process.

Results and discussion

Experimental design

We started our study from the design of the experimental setup and the selection of relevant conditions for the estimation of thermal and non-thermal effects of a plasmon. First of all, we chose an alkoxyamine as a chemical probe owing to the vast information about the thermal decomposition of these compounds.[33–37] Thermal homolysis of alkoxyamines $R_1R_2NOR_3$ leads to the formation of alkyl $R_3^{\bullet}$ and nitroxyl $R_1R_2NO^{\bullet}$ radicals, which are readily monitored by EPR spectroscopy. For the careful estimation of plasmon effects, alkoxyamine moieties should be located in the vicinity of the plasmonic surface, where the thermal effects will be the most pronounced. In order to solve this issue, we prepared alkoxyamines bearing $-NH_2$

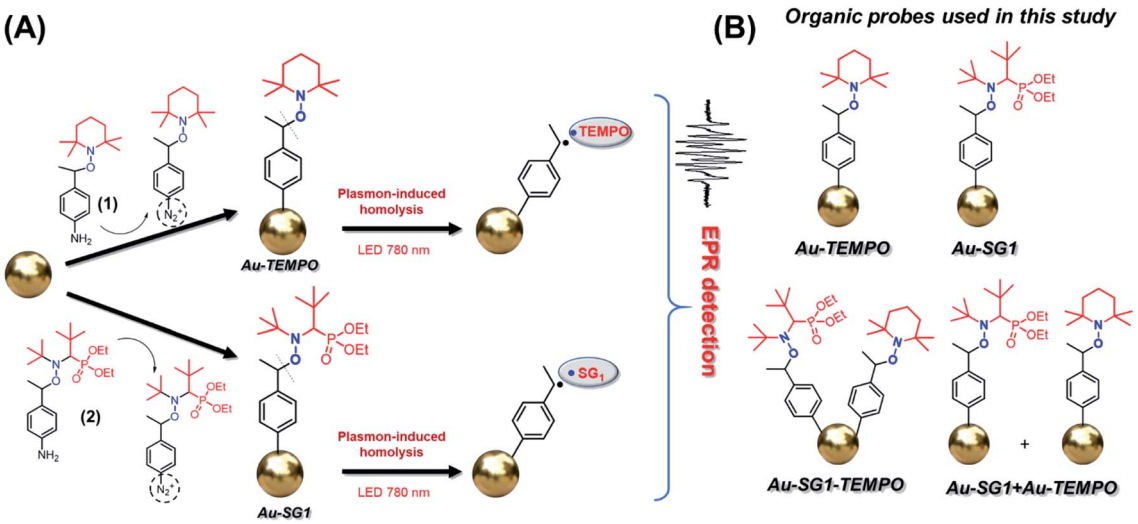

Fig. 2 (a) Au–TEMPO and Au–SG_1 preparation by diazotation/modification and plasmon-induced homolysis. (b) Schematic representation of Au–TEMPO, Au–SG_1, Au–SG_1–TEMPO, and Au–SG_1 + Au–TEMPO.

groups for the diazotization and subsequent covalent attachment (Fig. 2a) directly to AuNPs. Alkoxyamines **1** (TEMPO) and **2** (SG_1) (Fig. 2a) were prepared according to a reported procedure,[38] and their diazotization was performed in methanol, affording the corresponding arenediazonium salts.

The covalent attachment of alkoxyamine to AuNPs was realized through the simple addition of a freshly prepared suspension of AuNPs to the solution of the prepared diazonium salts. We also prepared AuNPs containing both alkoxyamine moieties **Au–SG_1–TEMPO** (Fig. 2b) *via* a preliminary diazotization of (**1**) and (**2**) and their mixing and addition to AuNPs (for details see experimental procedures in ESI and SN5†).

In comparison with traditional thiol-based approaches, relying on the utilization of Au–S bonds,[39,40] covalent attachment of aryl groups *via* Au–C bonding is significantly more stable, especially under heating.[39–41] Thus, the covalent attachment of alkoxyamine (**1**) and (**2**) moieties allows precise determination of the effect of plasmon excitation on the homolysis rate without the aforementioned disadvantages (Fig. 1).

As mentioned above, the homolysis rate and, more importantly, kinetic parameters are dependent on the structure of the organic probe. It means that the direct comparison of reaction kinetics of **Au–TEMPO** and **Au–SG_1** under similar experimental conditions will provide a possibility to directly estimate the thermal and non-thermal contribution of the plasmon to the kinetic parameters. In order to avoid any possible experimental deviations, we suggest applying four types of probes – **Au–TEMPO**, **Au–SG_1** and their mixture and **Au–SG_1–TEMPO**, where both organic functional groups are distributed across AuNPs and can be homolyzed under the same conditions. Moreover, such a design allows us to introduce additional control on the reproducibility of kinetic measurements.

Thus, we conceptualized the experimental design to estimate the thermal and non-thermal effects of plasmons on the alkoxyamine homolysis (Fig. 3). The detailed description of the experimental setup is given as ESI Note 1 (SN1).†

Briefly, AuNPs were dispersed in the *tert*-butylbenzene as a nonpolar solvent for EPR[42] treated by ultrasonication to obtain a homogeneous dispersion. The prepared samples were measured by EPR to obtain blank spectra. Then, the AuNP suspension was irradiated with an LED with the wavelength corresponding to the maximum of plasmon resonance of AuNPs in *tert*-butylbenzene. After irradiation for definite periods, the EPR spectra were recorded, providing information about the nature (pattern of signal) and amount of radicals (intensity). Furthermore, the AuNP suspension was again sonicated and irradiated, and EPR spectra were recorded. Repeating this operational sequence provided the kinetic curves, affording kinetic parameters for plasmon-induced homolysis of alkoxyamines.

Characterization of surface-modified gold nanoparticles (Au–TEMPO, Au–SG_1, and Au–SG_1–TEMPO)

AuNPs prepared (Fig. S1, SN2†) by chemical reduction[43] were modified with alkoxyamines (**1**) and (**2**) *via* diazonium chemistry with the formation of covalently grafted moieties. The as-prepared AuNPs (average diameter 13.5 ± 2.1 nm) demonstrate the maximum of plasmon resonance in water at 518 nm (Fig. 4, S1B and C†).

After modification with alkoxyamines (**1**) and (**2**), the resulting AuNPs (**Au–TEMPO**, **Au–SG_1**, **Au–TEMPO–SG_1**, and **Au–SG_1–TEMPO**) have been carefully washed with water and methanol (sodium citrate was removed) and transferred to the *tert*-butylbenzene *via* solvent exchange (for details, see the experimental part and Fig. S2–S6 and SN2–SN6†) for further experiments.

The attachment of organic functional groups has been confirmed by Raman spectroscopy and X-ray photoelectron spectroscopy (XPS). Surface-Enhanced Raman Spectroscopy (SERS) data (Fig. 4A, S3–S6†) highlight the appearance of peaks related to the attached alkoxyamines **1** and **2** (the full assignment of peaks is provided in Table S1†). SERS spectra of **Au–SG_1–TEMPO** and **Au–SG_1** + **Au–TEMPO** display the typical pattern of peaks for alkoxyamines (**1**) and (**2**), *i.e.*, aromatic ring, P=O stretching, C–N stretching and alkyl vibrations in the region 300–1700 cm^{-1} and, more importantly, Au–C stretching at 380–390 cm^{-1} (see Fig. S4b, S5b, Table S1 for details†). The position of peaks is almost identical as in the case of separate grafting of alkoxyamines (**1**) and (**2**). The position of "Ar ring str" peaks for **Au–SG_1** + **Au–TEMPO** is slightly shifted compared to **Au–SG_1** and **Au–TEMPO** (1589 cm^{-1} *vs.* 1598 cm^{-1}) accompanied by general peak broadening of spectra due to the preparation procedure and poor SERS reproducibility for AuNPs.

XPS spectra revealed an increase in C 1s (284.8 eV), O 1s (532.7 eV), and N 1s (400 eV) simultaneously with a decrease in

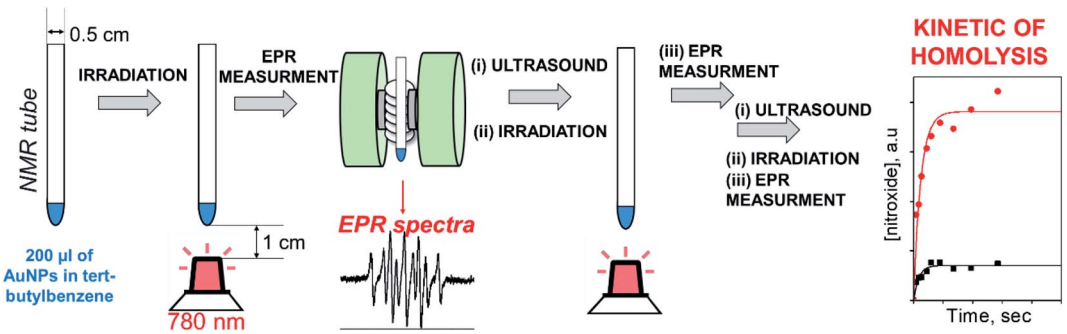

Fig. 3 Experimental setup of this work.

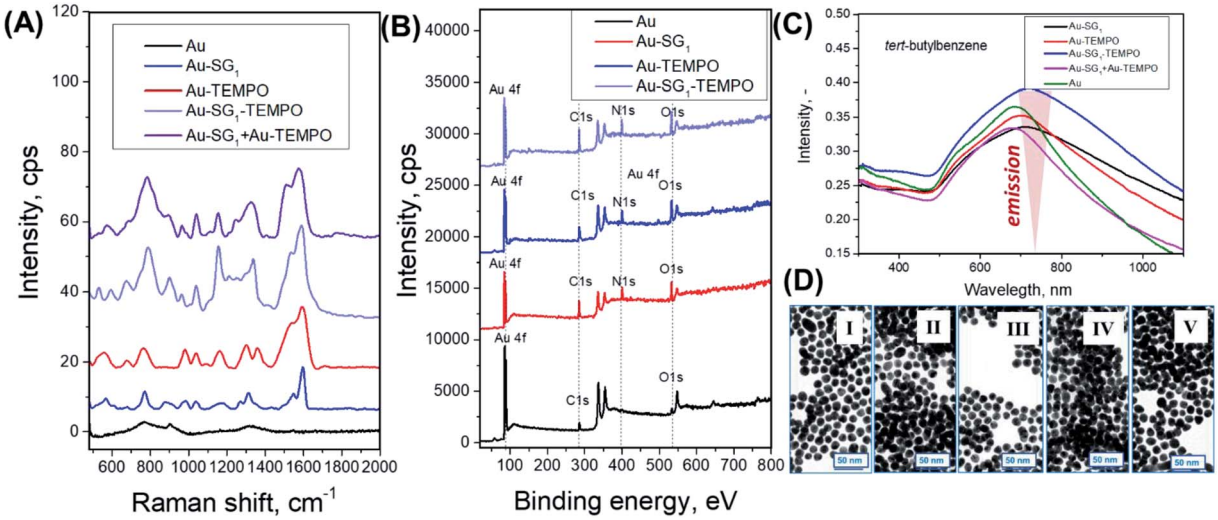

Fig. 4 Characterization of AuNPs functionalized with alkoxyamines. (A) SERS spectra at 785 nm wavelength (peak assignment in Table S1†) measured from AuNPs deposited on silicon, (B) survey XPS spectra (position of peaks are described in text), (C) UV-Vis spectra in *tert*-butylbenzene measured before experiments, and (D) transmission electron microscopy images (I -AuNPs, II-**Au–SG$_1$**, III-**Au–TEMPO**, IV-**Au–SG$_1$–TEMPO**, V- **Au–SG$_1$** + **Au–TEMPO**).

the Au 4f (85.2–88.8 eV) peak intensities because of the attachment of the organic moieties and screening of the gold surface (Fig. 4B, S2–S5C†). The attenuation of the Au signal enabled us to calculate the thickness of the alkoxyamine layer and surface coverage: 2.1 nm and 2.7 molecules per nm^2 for **Au–SG$_1$**; 1.8 nm and 5.7 molecules per nm^2 for **Au–TEMPO**; and 1.4 nm and 2.8 molecules per nm^2 for **Au–SG$_1$–TEMPO** (SN7†). The obtained values are within one order of magnitude and confirmed the presence of 1–2 phenylene layers of grafted alkoxyamines. A photoemission spectrum of the N(1s) line is shown in Fig. S6,† where the peaks ascribed to N–O bonds are detected similarly to those reported previously for TEMPO[44] and SG$_1$ (ref. [31]) moieties grafted on surfaces. Accordingly, the combination of Raman spectroscopy and XPS proves the successful grafting of alkoxyamines to AuNPs.

The optical characterization was performed by UV-Vis measurement in water and *tert*-butyl benzene (Fig. 4C, S2–S5D†). UV-Vis spectra in water display the broadening and shift of peak after modification: maximum ≈690 nm for **Au–SG$_1$**; maximum ≈675 nm for **Au–TEMPO**; maximum ≈695 nm for **Au–SG$_1$–TEMPO**; and maximum ≈665 nm for **Au–SG$_1$** + **Au–TEMPO** (Fig. S2–S5D†). Transfer of AuNPs to *tert*-butylbenzene leads to the appearance of peaks with the maximum at 715 nm for **Au–SG$_1$**; 705 nm for **Au–TEMPO**; 720 nm for **Au–SG$_1$–TEMPO**; and 705 nm for **Au–SG$_1$–TEMPO** (Fig. 4C, S2–S5E, SN2-SN6†). This broadening of peaks is because of the approaching of AuNPs to each other and some aggregation. A dominant dipole feature is observed that is pushed into the infrared due to interparticle coupling or increased light scattering.[45,46] These changes in AuNP approach and agglomeration are also evident from TEM images (Fig. 4D, S2–S5E†), where the average size of AuNPs almost did not change (Fig. S2–S5G†).

To calculate alkoxyamine loading and the amount of AuNPs, CHNS elemental analysis (EA) with atomic absorption spectroscopy (AAS, measurement error 0–10%) was implemented. The change in nitrogen content after modification was used to calculate the alkoxyamine loading in mmol per g of AuNPs. The elemental composition of the grafted alkoxyamines groups allowed us to establish a molar amount of functional groups per 1 g of AuNPs. The following values were obtained: 0.08 mmol g^{-1} **Au–SG$_1$** ([Au] = 6.7 mg L^{-1}); 0.087 mmol g^{-1} for **Au–TEMPO** ([Au] = 7.1 mg L^{-1}); and 0.083 mmol g^{-1} for **Au–SG$_1$–TEMPO** ([Au] = 9.2 mg L^{-1}) (Fig. S2–S5G and SN2-SN6†).

The following basic parameters were carefully registered before utilization of AuNPs in the plasmon-induced or thermal homolysis: absorption coefficient (UV-Vis), [Au] concentration (AAS), alkoxyamine loading (EA), and surface coverage (XPS) (Fig. S2–S5G†). Comparison of these basic parameters for **Au–SG$_1$**, **Au–TEMPO**, **Au–SG$_1$–TEMPO**, and **Au–SG$_1$** + **Au–TEMPO** does not show a significant difference (Fig. 4, S2–S5G†). All discrepancies are taken into account as inconsiderable for kinetic study. The broadening of the plasmonic peak of AuNPs appears to be almost identical so that these parameters can be disregarded for the evaluation of plasmonic behavior, and further detailed study will be devoted to the chemical reactivity under plasmon excitation and heating.

Homolysis of Au–SG$_1$, Au–TEMPO, and Au–TEMPO–SG$_1$

With the modified AuNPs in hand, we started to investigate the homolysis of **Au–SG$_1$**, **Au–TEMPO**, and **Au–TEMPO–SG$_1$** under two conditions: external heating and light-emitting diode (LED) irradiation at 25 °C with a wavelength (λ) of 780 nm (7 mW mm^{-2}) (corresponding to the plasmon absorbance band, Fig. 4C).

The typical patterns for the EPR signal of TEMPO and SG$_1$ (Fig. 5a, Table 1) present the 6- and 3-line patterns (X axis), respectively and are marked by stars and circles. The intensity changes (Y axis) of EPR signals from TEMPO and SG$_1$ radicals

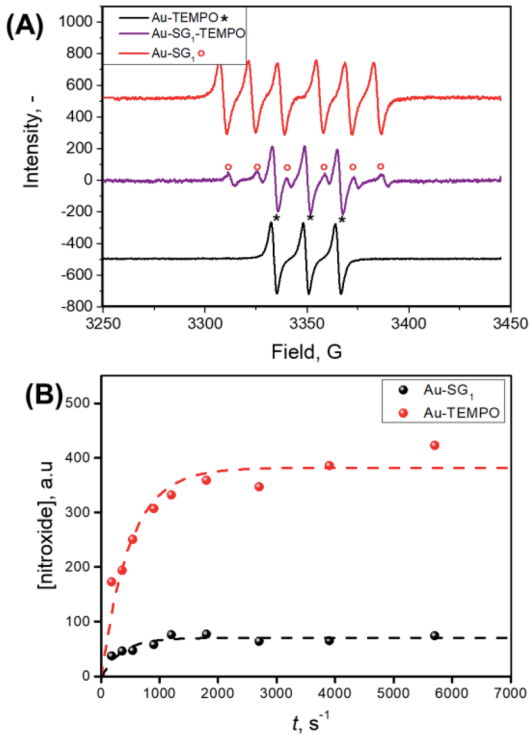

Fig. 5 Illustrative EPR results (A) The EPR signal of Au–TEMPO, Au–SG_1, and Au–SG_1–TEMPO (entry 7) after 95 min of irradiation. Stars and circles indicate the 3-line EPR signal of TEMPO, and the 6-line EPR signal of SG_1, respectively. (B) EPR kinetics for entry 7 in Table 1. The curves are exponential fits of eqn (1).

afford easy monitoring of the released nitroxide by EPR under plasmon irradiation. The signal from **Au–SG_1–TEMPO** also displays well-defined EPR patterns (Fig. 5A). The growth in the EPR signal of the corresponding released nitroxides affords first-order kinetic curves for all processes (Table 1, Fig. 1, S7†). The values of k_d (Table 1, S2†) are estimated by fitting the plots of concentration *vs.* time with eqn (1) (Fig. S7,† Fig. 5b).

$$k_d = [\text{nitroxide}]_\infty(1 - e^{-kt}) \quad (1)$$

Upon irradiation of **Au–SG_1** and **Au–TEMPO** with an LED with 780 nm wavelength, we noted fast growth of radical concentration in the first 300–400 s (Fig. 5B, entries 3 and 5, Table 1), and a plateau of nitroxide concentration was reached in less than 10 000 s, meaning that all alkoxyamine decomposed in sharp contrast to the expected result of thermal homolysis. It should be noted that the amount of released radical is equal to the molar loading of alkoxyamines on AuNPs. The EPR-derived concentration of alkoxyamines perfectly converges with data of EA and AAS, which proves the full conversion of homolysis (Fig. S2–S5G and SN2–6†). Full conversion of the attached alkoxyamines was additionally confirmed by SERS (Fig. S9 and SN9†). Thus, we observed the disappearance of characteristic bands of NO–C bonds near 1300 cm^{-1} and the emergence of a vibrational band at 1646–1666 cm^{-1} associated with C=O bonds after interaction with atmospheric oxygen. For both **Au–SG_1** and **Au–TEMPO**, the experiments were conducted in duplicate using two different batches of nanoparticles and showed good reproducibility for the amount of released nitroxides and k_d values (see Table S2†). To prove the plasmonic nature of the homolysis, we performed additional experiments in the dark with **Au–SG_1** (entry 9, Table 1) and under irradiation by an LED with 340 nm emission wavelength (2 mW mm^{-2}) (entry 8, Table 1). In both cases, only traces of nitroxides were detected after 1000 s. It should be noted that 340 nm wavelength is overlapped with the absorbance of pristine alkoxyamine (**2**) (SG1-substituted, Fig. S10†), which excludes the possible photoactivation pathway and highlights the plasmonic nature of the homolysis process.

As mentioned above, assuming a pure thermal effect of plasmon excitation, T_p was found to be *ca.* 91 and *ca.* 113 °C for **Au–SG_1** (entry 5, Table 1) and **Au–TEMPO** (entry 3, Table 1), respectively. Hence, considering that the reaction proceeded at 25 °C, the obtained values are 66 and 88 °C for **Au–SG_1** and **Au–TEMPO**, respectively, which could account for the results. As all

Table 1 Experimental results of the homolysis of **1**, **2**, Au–TEMPO Au–SG_1, and Au–TEMPO–SG_1 (details of kinetic parameters calculations are in Fig. S11 (see ESI))

Entry	Material	T^a (°C)	$k_d{}^b$ (10^{-4} s^{-1})	$E_a{}^c$ (kJ mol^{-1})	$T_p{}^d$ (°C)
1	**1**	99	3.3	127.3	[e]
2	**Au–TEMPO**	90–131	[f]	127.9[g]	[e]
3	**Au–TEMPO**	25, PI	12.5	[e]	113
4	**2**	[h]	[h]	124.5	[e]
5	**Au–SG_1**[e]	90–120	[i]	119.4[g]	[e]
6	**Au–SG_1**	25, PI	19.0	[e]	91
7	**Au–TEMPO–SG_1**	25, PI	28.8 (SG_1)	[e]	96 (SG_1)
			20.6 (TEMPO)		118 (TEMPO)
8	**Au–SG_1**[j]	25, 340 nm	—	—	—
9	**Au–SG_1**[j]	25, dark	—	—	—

[a] Temperature observed in the EPR cavity. PI = plasmon-induced. [b] Error of k_d is less than 10%. [c] Error of E_a is assumed as 2 kJ mol^{-1}. [d] Estimated T_p assuming a pure thermal effect for the plasmon effect. [e] Not determined. [f] At 90 °C, k_d values are 0.00014 to 0.00008 s^{-1} depending on the batch of nanoparticles. [g] Averaged values of all (4) measurements. [h] See ref. [34]. [i] At 90 °C, k_d varies from 0.00092 to 0.0059 s^{-1} depending on the batch of nanoparticles. [j] Control experiments – kinetics obtained in the dark (no plasmon excitation) and kinetics obtained under irradiation by an LED with 340 nm emission wavelength – displayed only traces of nitroxides on the threshold level after 1000 s of experiments.

the samples received the same energy from the LED sources (780 nm, 7 mW mm^{-2}), the same plasmon effect was expected for both **Au–SG$_1$** and **Au–TEMPO**. Nevertheless, we observed a noticeable ~22 °C difference in experimental T_p, which proves the contribution of non-thermal effects (Fig. S11 and SN11†).

First, we estimated values of k_d for thermal homolysis of (**1**), **Au–TEMPO**, (**2**), and **Au–SG$_1$** and the corresponding activation energy E_a (eqn (2)), using the previously reported averaged factor $A = 2.4 \times 10^{14}$ s^{-1}.[34] *para*-Substituted aryl alkoxyamines containing TEMPO and SG_1 moieties have been extensively investigated, which allows determining the effects of AuNPs on the reaction kinetics.[38,47] In general, the presence of electron-donating groups (EDGs) (such as Au metal) should slightly decrease k_d or display a weak effect on k_d (delta $E_a \approx 0.6$ kJ mol^{-1}) as observed for **1** and **Au–TEMPO**[47] (entries 1, 2, 4, and 5; Table 1). However, these changes are more striking for **Au–SG$_1$** than for **Au–TEMPO**. Indeed, the decrease of *ca.* 5 kJ mol^{-1} observed for **Au–SG$_1$** is associated with electronic effects due to the covalent aryl–gold bond formation (Fig. S8 and SN7†). According to the literature, EDGs or atoms (such as gold) may lead to a decrease of k_d in sharp contrast to the observed results[48].

We tentatively ascribe this phenomenon to the back donation of π-electrons in empty d (as displayed in Fig. S8† as an example) and f orbitals of an Au atom favoring an increase in the partial positive charge at the *ipso*-position of the aryl moiety (details of the observed phenomenon are provided in Fig. S8 and SN8†).

Estimation of kinetic parameters for Au–SG$_1$ and Au–TEMPO

The values of E_a (constant for **Au–SG$_1$** and **Au–TEMPO** independent of reaction conditions) allowed us to estimate the most important parameter of the non-thermal (or thermal) contribution of the plasmon to the homolysis of an alkoxyamine: apparent temperature T_p of homolysis (eqn (3) and Table 1, SN11†). Assuming that the homolysis is mediated solely by the thermal effect of plasmon excitation, the T_p value should be equal to the temperature of homolysis under heating. Any difference in Tp speaks by itself in temperatures speaks by itself and makes it possible to estimate the non-thermal contribution *via* temperature difference and the related kinetic parameters.

$$E_a = RT \ln\left(\frac{A}{k_d}\right) \quad (2)$$

$$T_p = -\frac{E_a}{R \ln(A/k_d)} \quad (3)$$

Estimation of kinetic parameters for Au–TEMPO–SG$_1$ and Au–SG$_1$ + Au–TEMPO

To circumvent any issues due to the setup, the procedure, and the effect of the surface modification, we prepared AuNPs **Au–TEMPO–SG$_1$** containing both alkoxyamines (**1**) and (**2**) (Fig. S4, SN5†) with the same amount of covalently grafted alkoxyamines as for pure **Au–SG$_1$**, **Au–TEMPO** (Fig. S2–S4†). In the presence of both alkoxyamines on the surface, the expected increase of radical concentrations (SG_1 and TEMPO) was observed (Fig. 5B) under illumination. Estimated T_p values (entry 7, Table 1) were found to be very similar to those for pure **Au–SG$_1$** and **Au–TEMPO**. In this case, the energy of the plasmon interacting with both attached alkoxyamines on AuNPs is the same. The difference in T_p between SG_1 (96 °C) and TEMPO (118 °C) is ascribed only to a specific interaction of the plasmon with grafted alkoxyamines, highlighting the non-thermal effects and strict dependencies on the structure of alkoxyamine. As additional evidence, similar kinetic parameters have been observed for the homolysis of **Au–SG$_1$** + **Au–TEMPO** (Fig. S5, SN6 and 10†) in solution (Table S2,† entries 7 and 8). Hence, assuming that the homolysis of **Au–SG$_1$** proceeded due to a pure thermal effect, **Au–TEMPO** should also display a T_p equal to 96 °C (the same as for **Au–SG$_1$**), affording an E_a of 120.6 kJ mol^{-1}. Nevertheless, the calculated T_p for **Au–TEMPO** was sufficiently larger (118 °C), which gives at least a 7.6 kJ mol^{-1} gain of energy related to plasmon excitation (Fig. S10 and SN11†) calculated from the kinetic parameters obtained under external heating (entries 2 and 5) and plasmon-induced homolysis (entries 3 and 6).

A question still arises about the importance of thermal heating of the surface under plasmon irradiation. The temperature of the experimental system can be decomposed into macroscopic collective effects, measurable with a thermometer, and local overheating of nanoparticles, calculated theoretically. Performed calculations revealed that under our experimental conditions, local heating in the vicinity of AuNPs is on the order of 10^{-3} °C (Fig. S11 and SN12†). It is interesting to estimate the LED power density needed to achieve the local temperature elevation of 66 °C, under the assumption of a pure thermal effect for the homolysis of **Au–SG$_1$**. By numerically solving the corresponding equation, we found that such heating is reached under an illumination of $\sim 5.02 \times 10^8$ J m^{-2} in contrast to 7 J m^{-2} utilized in our experiments, which is 10^8-fold less. Consequently, calculations support the fact that the local heating effects at the surface are negligible. Additional experiments with temperature tracking using a miniaturized leaf thermocouple immersed in the AuNP suspension revealed the increase of the suspension temperature by <1.5 °C within the error bar after 30 minutes of irradiation (Fig. S12 and SN13†) under the above-stated experimental conditions, ruling out the possible thermal homolysis (taking into account homolysis temperatures larger than 60 °C) during irradiation of the sample.

Plausible mechanisms of plasmon-induced homolysis of alkoxyamines

As described previously, the homolysis of C–I or S–S bonds can proceed without the involvement of hot carriers *via* intrinsic excitation of an electron to the LUMO followed by decomposition.[19,49] In our opinion, the cleavage of alkoxyamines can be initiated by a similar mechanism (Fig. 6A). The plasmon energy can induce intramolecular excitation and formation of a dissociative transition state (TS), which can be spontaneously decomposed with the formation of two radicals. The pathway associated with the ionization of molecules by hot carriers

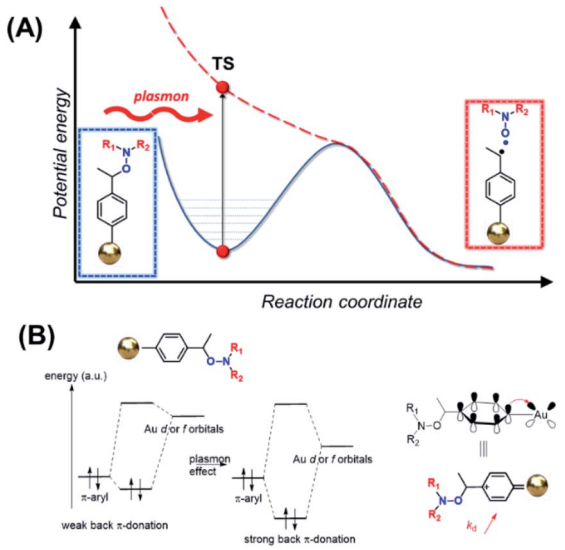

Fig. 6 Tentative mechanisms. (A) Tentative mechanism of plasmon-induced homolysis of **Au–SG$_1$/TEMPO**. (B) Back π-donation of a π-electron of the aromatic ring into empty d or f orbitals of an Au atom accounting for the increase in k_d.

seems to be less possible due to the formation of cationic or anionic species, which have not been detected by EPR spectroscopy. Moreover, the energy required for the homolysis of covalently attached alkoxyamine could be sufficiently lowered by back π-donation, as was mentioned before for the thermal homolysis (Fig. S8B†). This phenomenon can be explained by the interaction between empty d and f orbitals of gold with the π-electrons, which should increase the partial positive charge at the *ipso* position (loss of electron density in the π-cloud). The back π-donation causes an increase in electronegativity of the C atom of the C–O bond, thereby weakening this bond, as commonly observed for chemical triggering of C–ON bond homolysis.

Conclusions

In conclusion, in contrast to commonly used probes for mechanistic studies of plasmonic reactions, we demonstrated the applicability of alkoxyamines covalently grafted to AuNPs for the well-defined kinetic study (due to one component reaction with 1st order kinetics) of their homolysis under plasmon excitation using EPR monitoring. Experimentally obtained kinetic parameters of homolysis, especially T_p, calculated assuming a solely thermal contribution, enable us to quantify the unquestionable presence of a non-thermal component. Experiments with the homolysis of **Au–SG$_1$–TEMPO** and **Au–TEMPO** + **Au–SG$_1$**, where the amount of energy delivered by an LED is equal for both alkoxyamines, reveal a considerable difference in T_p. The observed difference of 22 °C confirms that the effects of the plasmon are explicitly attributable to the nature of the organic molecule. As a result, our study highlights the presence of a non-thermal plasmon effect and moves us closer to the understanding of the nature of the plasmon interaction with organic molecules. The observed results indicate that the structure of organic molecules and the nature of chemical transformation should be considered for plasmon catalysis. A further mechanistic study using plasmonic substrates and organic molecules should be addressed from both physical and chemical points of view for full understanding. To date, several questions are still pending: what is the strength of each effect? Can the plasmon effect be tuned by the reaction conditions? At this time, our data do not allow the size of each component to be quantitated. Nevertheless, we believe that our findings will shed light on the mechanisms of the plasmon-assisted reaction and will prompt scientists to develop novel plasmon-initiated transformations.

Author contributions

Olga Guselnikova: preparation and characterization of the materials, conducting the experiments, and writing of the manuscript; Andrey Trelin: the simulations; Gérard Audran: manuscript revision and proofreading; Jean-Patrick Joly: preparation of the alkoxyamines; Evgeny V. Tretyakov: study conception, design of the experiments, and proofreading; Vaclav Svorcik: manuscript revision and proofreading; Oleksiy Lyutakov: analysis of the data; Sylvain R. A. Marque: study conception, design of the experiments, analysis of the data, and writing of the manuscript; Pavel Postnikov: study conception, design of the experiments, analysis of the data, and writing of the manuscript.

Conflicts of interest

There are no conflicts to declare.

Acknowledgements

The authors acknowledge the Tomsk Polytechnic University Competitiveness Enhancement Program in frame of project VIU-RSCABS-194/2020 and the GACR under the project 20-01768S.

Notes and references

1 X. Zhang, X. Ke and J. Yao, *J. Mater. Chem. A*, 2018, **6**, 1941.
2 S. Linic, U. Aslam, C. Boerigter and M. Morabito, *Nat. Mater.*, 2015, **14**, 567.
3 C. Zhan, X. J. Chen, J. Yi, J. F. Li, D. Y. Wu and Z. Q. Tian, *Nat. Rev. Chem.*, 2018, **2**, 216.
4 H. H. Shin, J. J. Koo, K. S. Lee and Z. H. Kim, *Appl. Mater. Today*, 2019, **16**, 112.
5 S. K. Cushing and N. Wu, *J. Phys. Chem. Lett.*, 2016, **7**, 666.
6 X. Meng, L. Liu, S. Ouyang, H. Xu, D. Wang, N. Zhao and J. Ye, *Adv. Mater.*, 2016, **28**, 6781.
7 Q. Yang, Q. Xu, S.-H. Yu and H.-L. Jiang, *Angew. Chem., Int. Ed.*, 2016, **55**, 3685.
8 M. Wen, S. Takakura, K. Fuku, K. Mori and H. Yamashita, *Catal. Today*, 2015, **242**, 381.

9 O. Guselnikova, P. Postnikov, M. M. Chehimi, Y. Kalachyovaa, V. Svorcik and O. Lyutakov, *Langmuir*, 2019, **35**(6), 2023.
10 R. M. Sarhan, W. Koopman, R. Schuetz, T. Schmid, F. Liebig, J. Koetz and M. Bargheer, *Sci. Rep.*, 2019, **9**, 1.
11 Y. Sivan, I. W. Un and Y. Dubi, *Chem. Sci.*, 2019, **19**, 45.
12 L. Zhou, D. F. Swearer, C. Zhang, H. Robatjazi, H. Zhao, L. Henderson, L. Dong, P. Christopher, E. A. Carter, P. Nordlander and N. J. Halas, *Science*, 2018, **362**, 69.
13 Y. Sivan, J. Baraban, I. W. Un and Y. Dubi, *Science*, 2019, **364**, eaaw9367.
14 L. Zhou, D. F. Swearer, H. Robatjazi, A. Alabastri, P. Christopher, E. A. Carter, P. Nordlander and N. J. Halas, *Science*, 2019, 364.
15 J. J. Baumberg, *Faraday Discuss.*, 2019, 501–511.
16 Y. Sivan, I. W. Un and Y. Dubi, *Faraday Discuss.*, 2019, 215–233.
17 Y. Dubi and Y. Sivan, *Light: Sci. Appl.*, 2019, **8**, 1.
18 X. Zhang, X. Li, M. E. Reish, D. Zhang, N. Q. Su, Y. Gutiérrez, F. Moreno, W. Yang, H. O. Everitt and J. Liu, *Nano Lett.*, 2018, **18**, 1714.
19 E. Kazuma, J. Jung, H. Ueba, M. Trenary and Y. Kim, *Science*, 2018, **360**, 521.
20 Y. Sivan, I. W. Un and Y. Dubi, *Faraday Discuss.*, 2019, 215–233.
21 P. K. Jain, *J. Phys. Chem. C*, 2019, **123**, 24347.
22 G. V. Hartland, L. V. Besteiro, P. Johns and A. O. Govorov, *ACS Energy Lett.*, 2017, **2**, 1641.
23 J. Guo, Y. Zhang, L. Shi, Y. Zhu, M. F. Mideksa, K. Hou, W. Zhao, D. Wang, M. Zhao, X. Zhang, J. Lv, J. Zhang, X. Wang and Z. Tang, *J. Am. Chem. Soc.*, 2017, **139**, 17964.
24 Q. Yang, Q. Xu, S.-H. Yu and H.-L. Jiang, *Angew. Chem., Int. Ed.*, 2016, **55**, 3685.
25 P. S. Jain, *Chem. Sci.*, 2020, **11**, 9022.
26 Z. Li, Y. Gao, L. Zhang, Y. Fang and P. Wang, *Nanoscale*, 2018, **10**, 18720.
27 E. L. Keller and R. R. Frontiera, *ACS Nano*, 2018, **12**(6), 5848.
28 H. Kookhaee, T. E. Tesema and T. G. Habteyes, *J. Phys. Chem. C*, 2020, **124**(41), 22711.
29 T. Chen, F. Tong, J. Enderlein and Z. Zheng, *Nano Lett.*, 2020, **20**(5), 3326.
30 W. Koopman, R. M. Sarhan, F. Stete, C. N. Z. Schmitt and M. Bargheer, *Nanoscale*, 2020, **12**(48), 24411–24418.
31 O. Guselnikova, S. R. A. Marque, E. V. Tretyakov, D. Mares, V. Jerabek, G. Audran, J. P. Joly, M. Trusova, V. Svorcik, O. Lyutakov and P. Postnikov, *J. Mater. Chem. A*, 2019, **7**, 12414.
32 J. Nicolas, Y. Guillaneuf, C. Lefay, D. Bertin, D. Gigmes and B. Charleux, Nitroxide-mediated polymerisation, *Prog. Polym. Sci.*, 2013, **38**, 63.
33 D. Bertin, D. Gigmes, S. R. A. Marque and P. Tordo, *Chem. Soc. Rev.*, 2011, **40**, 2189.
34 *Encyclopedia of Radicals in Chemistry, Biology and Materials*, ed. C. Chatgilialoglu and A. Studer, John Wiley & Sons, Ltd, Chichester, UK, 2012.
35 E. G. Bagryanskaya and S. R. A. Marque, *RSC Polym. Chem. Ser.*, 2016, 45–113.
36 M. V Edeleva, S. R. A. Marque and E. G. Bagryanskaya, *Russ. Chem. Rev.*, 2018, **87**, 328.
37 M. Edeleva, G. Audran, S. Marque and E. Bagryanskaya, *Materials*, 2019, **12**, 688.
38 G. Audran, P. Brémond, J. P. Joly, S. R. A. Marque and T. Yamasaki, *Org. Biomol. Chem.*, 2016, **14**, 3574.
39 D. M. Shewchuk and M. T. McDermott, *Langmuir*, 2009, **25**(8), 4556.
40 L. Civit, A. Fragoso and C. K. O'Sullivan, *Electrochem. Commun.*, 2010, **12**(8), 1045.
41 L. Laurentius, S. R. Stoyanov, S. Gusarov, A. Kovalenko, R. Du, G. P. Lopinski and M. T. McDermott, *ACS Nano*, 2011, **5**, 4219.
42 D. Marsh, *J. Magn. Reson.*, 2008, **190**(1), 60.
43 J. Kimling, M. Maier, B. Okenve, V. Kotaidis, H. Ballot and A. Plech, *J. Phys. Chem. B*, 2006, **110**, 15700.
44 O. Guselnikova, P. Postnikov, S. R. A. Marque, V. Švorčík and O. Lyutakov, *Sens. Actuators, B*, 2019, **300**, 127015.
45 I. Romero, J. Aizpurua, G. W. Bryant and F. J. García De Abajo, *Opt. Express*, 2006, **14**, 9988.
46 L. Schumacher, J. Jose, D. Janoschka, P. Dreher, T. J. Davis, M. Ligges, R. Li, M. Mo, S. Park, X. Shen, S. Weathersby, J. Yang, X. Wang, F. Meyer Zu Heringdorf, K. Sokolowski-Tinten and S. Schlücker, *J. Phys. Chem. C*, 2019, **123**, 13181.
47 S. Marque, H. Fischer, E. Baier and A. Studer, *J. Org. Chem.*, 2001, **66**, 1146.
48 G. Audran, E. Bagryanskaya, I. Bagryanskaya, P. Brémond, M. Edeleva, S. R. A. Marque, D. Parkhomenko, E. Tretyakov and S. Zhivetyeva, *Inorg. Chem. Front.*, 2016, **3**, 1464.
49 E. Miliutina, O. Guselnikova, N. Soldatova, P. Bainova, R. Elashnikov, P. Fitl, T. Kurten, M. Yusubov, V. Švorčík, R. R. Valiev, M. Chehimi, O. Lyutakov and P. Postnikov, *J. Phys. Chem. Lett.*, 2020, **11**, 5770.